# Differential Gain Analysis of InGaAs/InGaAsP/InP Multiquantum Well Lasers with 1.55 $\mu$m Emission Wavelength

M.T. Furtado, W. Carvalho Jr., A.M. Machado and K. Jomori
*Centro de Pesquisa e Desenvolvimento,*
*Telecomunicações Brasileiras S/A-TELEBRÁS,*
*C.P.1579, 13088-061 Campinas, SP, Brazil*

Received June 5, 1997

We present measurements of the differential gain of multiquantum well (MQW) broad area lasers emitting at 1.55 $\mu$m wavelength, taking into account the nonuniform stimulated emission caused by filamentation within the optical cavity. The differential gain was determined from measurements of the threshold current density, considering the losses due to the inhomogenous carrier density distribution, as an apparent leakage current effect in the output power-current characteristics. The lasers were grown by low pressure MOCVD and incorporate an InGaAs/InGaAsP/InP separate confinement MQW active region. The results are compared with previous data reported on similar MQW heterostructures.

## I. Introduction

The differential gain, defined as the differential of the optical material gain to the increment of the injected carrier density, is an important material parameter of the active layer of semiconductor lasers [1,2]. The higher modulation bandwidths [3] as well as the lower wavelength chirp [4,5] observed in multiquantum well (MQW) lasers for the 1.55 $\mu$m emission wavelength range, are mainly a consequence, of the two dimensional density of energy states. The latter increases the differential gain of the MQW active layer relative to the bulk material. The differential gain is most often determined from measurements of the relaxation oscillation frequency as a function of the optical emitted power under the approximation of small signal modulation [3,5,6]. However, this technique has been shown to depend on the laser structure and, in addition, the frequency response is also limited at higher optical powers due to damping caused by saturation of the optical gain [7].

The differential gain is an intrinsic property of the material in the active layer and is independent of the laser structure and measurement technique. In a recent work, we have proposed a simple method to determine the differential gain in MQW broad area lasers from measurements of the threshold current density [8]. The broad area laser has one of the most simple device structure. It is generally used for the evaluation of the intrinsic properties of the active layer material, before undertaking the fabrication of more complicated laser structures. Nevertheless, the optical field resulting from the stimulated emission can be highly nonuniform due to the lack of lateral confinement, leading to a phenomenon known as filamentation. This has been recently reported in InGaAs/InGaAsP/InP MQW lasers [9]. In such cases, the stimulated emission occurs only around local regions along the laser cavity, although the current is injected uniformly below the large stripe width. Hence, the carrier density is inhomogenously distributed in the active layer and a significant fraction of the current injected between the laser electrodes generates only spontaneous emission. These losses affect the evaluation of the threshold current density and the external quantum efficiency from the laser output power- current ($P - I$) characteristics. An analogous behaviour has been reported recently for MQW ridge waveguide laser structures, where the optical gain was shown to be influenced by the existence of leakage currents outside the recombination region [10].

In this work, we have determined the differential gain of MQW broad area lasers, taking into account the carrier density losses produced by filamentation. We have treated the current losses in the active layer as an apparent leakage current effect in the $P-I$ characteristics. The laser devices were grown by metalorganic chemical vapor deposition (MOCVD), and comprised a separate confinement heterostructure (SCH) MQW active layer of lattice matched InGaAs/InGaAsP/InP emitting at 1.55 $\mu$m. In section II, we present the model employed to determine the differential gain including the carrier density losses derived from the $P-I$ characteristics. In section III, we briefly describe the MOCVD growth of the MQW laser structure as well as the device processing and characterization. In section IV, we analyse and discuss the results obtained and compare our data with previous results reported on similar MQW lasers. Finally, in section V, we present the conclusion.

## II. Basic assumptions and analysis

For a single QW layer, the optical material gain can be well approximated by a logarithmic function of the current density [11,12]

$$g = g_0 \ln \frac{\eta_i j}{j_0} \tag{1}$$

where $g_0$ is the gain coefficient, $\eta_i$ is the current injection efficiency into the QW layer, $j$ is the current density and $j_0$ is the current density at transparency. The threshold current density of a MQW laser with identical QWs is then obtained from the threshold condition where the gain equals the cavity losses, following the original derivation of Wilcox et al. [13], and it is given by the expression [8,11]:

$$j_{th} = \frac{N_Z j_0}{\eta_i} \exp\left(\frac{\alpha_i}{N_Z \Gamma_Z g_0}\right) \exp\left[\frac{1}{2 N_Z \Gamma_Z g_0 L} \ln\left(\frac{1}{R_1 R_2}\right)\right] \tag{2}$$

where $N_Z$ and $\Gamma_Z$ are the number of QWs and the optical confinement factor of a single QW, respectively, $R_1$ and $R_2$ are the mirror reflectivities, $\alpha_i$ is the absorption loss and $L$ is the cavity length. One notices that using the semi-logarithmic plot of $j_{th}$ versus the inverse of $L$, one easily obtains $g_0$ from the slope, since $N_Z$, $\Gamma_Z$ and $R_1(R_2)$ are known quantities for a given laser structure. However, $j_0$ cannot be simply determined from the intercept at the ordinate because $\eta_i$ and $\alpha_i$ must be found independently. In broad area lasers, $\eta_i$ can be assumed approximately equal to unity in equation (2), as long as the effects of carrier escape from the QWs as well as diffusion and recombination in the barrier and waveguide layers are neglected [14]. The value of $\alpha_i$ is usually extracted from the linear plot of the inverse external quantum efficiency as a function of $L$, given by the well known expression [11,12]

$$\frac{1}{\eta_{ext}} = \frac{1}{\eta_{id}} \left(1 + \frac{2\alpha_i L}{\ln \frac{1}{R_1 R_2}}\right) \tag{3}$$

Here $\eta_{id}$ represents the internal differential quantum efficiency defined as the ratio of the increase of emitted photons to the increase of injected carriers [15,16]. Its value is very close to one, because above threshold $\eta_{id}$ is dominated by stimulated emission, which is limited by the carrier intraband relaxation time [16,17]. Since the internal differential quantum efficiency depends on the current injection efficiency, we assume for simplicity in the following $\eta_{id} \approx \eta_i$, such that the current losses in the MQW active layer are considered to be limited only by the current injection efficiency. $j_{th}$ and $\eta_{ext}$ are evaluated from measurements of the threshold current and the differential efficiency, respectively, which are derived from the $P-I$ characteristics. Nevertheless, the results can be influenced by leakage currents in the laser structure [10,18], as well as by carrier escape and recombination in the waveguide layers of SCH-MQW lasers. The latter only lowers slightly $\eta_i$ at high current injection levels [19], but on lasers of very small cavity lengths, the resultant effect has been shown to be greater [20].

In contrast to previous works, we consider here the

inhomogeneous lateral distribution of the stimulated emission in broad area lasers produced by filaments, despite the uniform injected current below the wide stripe. Earlier work of Thompson [21] described filamentation arising from self-focusing effects in local regions of high emission intensity due to an increase of the refractive index as well as carrier depletion. Later, more elaborate models were proposed to explain the nonlinear interaction between the optical field and the refractive index, and conditions of stability for uniform laser emission under the laser stripe were determined [22,23]. According to previous work, filamentation in InGaAs/InGaAsP/InP MQW broad area lasers arise from local differences in the distribution of defects and/or dislocations in the active layer [9]. The isolated filaments may have different threshold currents, but their emission intensities are coupled by the same current source. The $P-I$ curve of the laser device is then the upper asymptote of the individual curves resulting from each filament [24]. The spontaneous emission generated by a significant fraction of the active layer cross section in the laser cavity, decreases the differential efficiency and increases the threshold current compared to a uniformily pumped broad area laser. Hence, as the injected current density increases in the active layer, the spontaneous emission also increases, and such behaviour is similar to that produced by a leakage current on the $P-I$ characteristics. So, we have assumed the spontaneous emission losses resulting from filamentation in the MQW active layer, as an apparent leakage current effect on the laser characteristics. The threshold current is then given by [10,18]:

$$I_{th} = wLj_{th} + I_l \tag{4}$$

where $w$ is the laser stripe width and $I_l$ is the leakage current. The latter increases with the total injected current $I$ in the device, and consequently, affects $j_{th}$ and the differential efficiency. If we assume a simple linear relationship, we may define a parameter $K = dI_l/dI$ which should be smaller than one, such that equation (4) can be written as

$$j_{th} = \frac{(1-K)I_{th}}{wL} \tag{5}$$

If one neglects the contribution of the spontaneous emission, the $P-I$ characteristic on each facet of the laser device is given by [18]

$$P = \frac{h\nu}{2e}\eta_{ext}(I - I_{th} - I_l) \tag{6}$$

Here $e$ is the elementary charge and $h\nu$ is the photon energy. Hence, by differentiation of equation (6) with respect to $I$, one obtains $\eta_{ext}$ as a function of the differential efficiency defined as $dP/dI$, including leakage current effects

$$\eta_{ext} = \frac{2e}{h\nu}\frac{1}{(1-K)}\frac{dP}{dI} \tag{7}$$

One notices that the factor $(1-K)$ appearing in equations (5) and (7) represents in fact the effective injection efficiency for stimulated emision in the active region. From the values of $I_{th}$ and $dP/dI$ measured on the $P-I$ curve for a given $L$, one obtains $j_{th}$ and $\eta_{ext}$ through equations (5) and (7), respectively. The value of $K$ is then adjusted so that the values of $\eta_i$ and $\alpha_i$ obtained from the plots of equations (2) and (3) as a function of $L$ can be matched. However, there is a limited range of established values for $g_0$, $j_0$, $\eta_i$ and $\alpha_i$ in InGaAs/InGaAsP/InP MQW lasers, so $K$ is the only unknown parameter that can be more freely adjusted for a given laser structure. Once $K$ is determined, one notices that the values of $j_{th}$ and $\eta_{ext}$ obtained from equations (5) and (7), respectively, correspond to their values within the filaments of the MQW active layer. These values are then used for the evaluation of the differential gain, as discussed in section IV.

The differential gain $dg/dn$ can be derived from equation (1) using an expression of $j$ in terms of the carrier density $n$. The latter is obtained from the carrier density rate equation neglecting stimulated emission and carrier diffusion [18], and one obtains [11]

$$j = \frac{eN_Z L_Z(An + Bn^2 + Cn^2)}{\eta_i} \tag{8}$$

where $L_Z$ is the thickness of a single QW layer. $A$, $B$ and $C$ are the nonradiative, the bimolecular (radiative) and the Auger recombination coefficients, respectively. However, we have recently demonstrated that a simpler and approximate expression may be used instead [8]

$$j = \frac{eN_Z L_Z B_{eff} n^b}{\eta_i} \tag{9}$$

where $B_{eff}$ is an effective recombination coefficient, which accounts for radiative as well as nonradiative transitions in the MQW active layer, and $b$ is in the range $2 \leq b \leq 3$. The parameters $B_{eff}$ and $b$ are adjusted such that equation (9) fits as close as possible equation (8) in a significant range of carrier densities. Previous investigators have attributed the values $b = 2$ and $B_{eff} = 1.4 \times 10^{-10}$ cm$^3$/s for bulk active layers of the InGaAsP/InP material system in the 1.55 $\mu$m emission wavelength range [25], assuming a given set of constants $A$, $B$ and $C$. If we assume the set of constants $A = 10^8$ s$^{-1}$, $B = 10^{-10}$ cm$^3$/s and $C = 10^{-28}$ cm$^6$/s, previously reported for InGaAs/InGaAsP/InP MQW layers [11,26], equation (8) can be fitted satisfactorily with $b = 2.55$ and $B_{eff} \approx 3 \times 10^{-20}$ cm$^{4.65}$/s in the range of $n = 1.5 \times 10^{18}$ cm$^{-3}$ and $5 \times 10^{18}$ cm$^{-3}$, which is of interest for laser devices [8]. Fig. 1 illustrates the good agreement obtained between equations (8) and (9) assuming the new values of $B_{eff}$ and $b$, where the normalised current density defined as $j/eN_ZL_Z$ is plotted versus $n$.

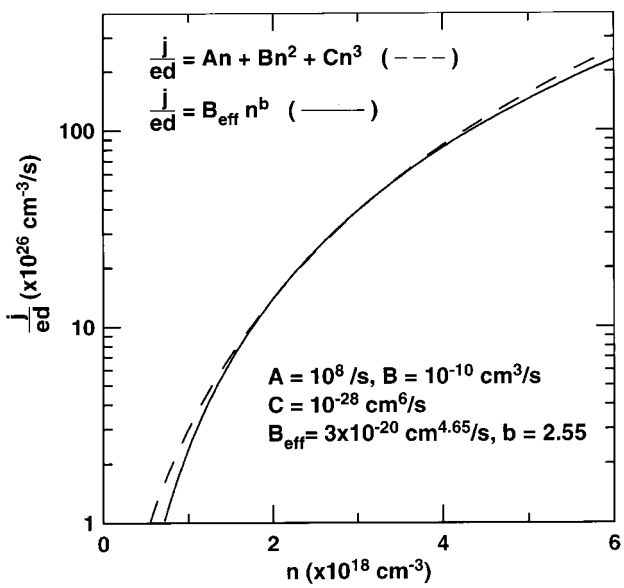


Figure 1. Plot of the normalised current density $j/ed$, where $d = N_ZL_Z$, versus carrier density assuming $\eta_i = 1$. Equation (9) with $B_{eff} = 3 \times 10^{-20}$ cm$^{4.65}$/s and $b = 2.55$ (solid line) and equation (8) with $A = 10^8$ s$^{-1}$, $B = 10^{-10}$ cm$^3$/s and $C = 10^{-28}$ cm$^6$/s (dotted line).

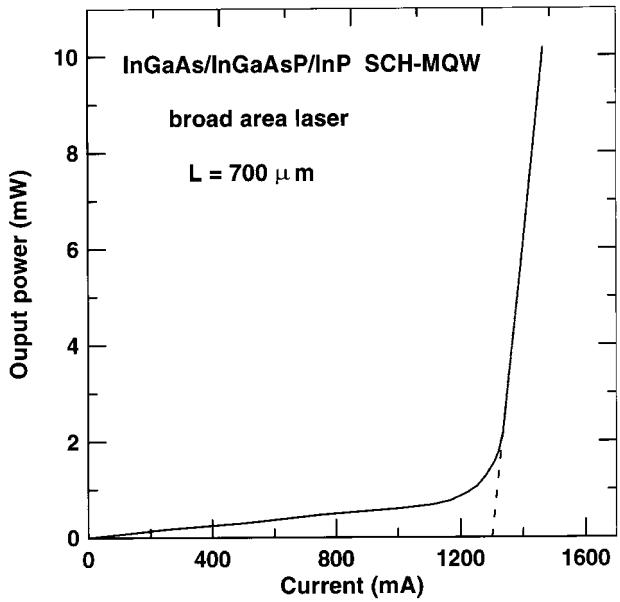


Figure 2. $P - I$ characteristic of a MQW broad area laser with $L = 700$ $\mu$m (solid curve). The dotted line represents equation (6).

Now, a simple relation for $g$ in terms of $n$ can be derived from equations (1) and (9), assuming $j_0 = eL_ZB_{eff}n_0b$, where $n_0$ is the carrier density at transparency. Note that $\eta_i$ does not appear in the definition of $j_0$, because we assume that only the injected carriers that contribute to the laser emission are included in the transparency current. Hence, we have

$$g = bg_0 \ln \frac{n}{n_0} \tag{10}$$

The differential gain is then given by the simple expression

$$\frac{dg}{dn} = \frac{bg_0}{n} \tag{11}$$

The values of $g_0$ and the threshold carrier density $n_{th}$ are determined from the semi- logarithmic slope of equation (2) and from equation (9) for a given value of $j_{th}$, respectively. These two equations are influenced by leakage currents in the $P - I$ characteristics through the value of $K$ in equation (5). However, the value determined for $dg/dn$ in equation (11) is mainly affected by $n_{th}$, which depends on the value of $j_{th}$, as discussed in section IV.

## III. Laser fabrication

The epitaxial heterostructure comprising the SCH-MQW active region was grown by low pressure

MOCVD on a $n^+$-InP substrate. The MQW consisted of 6 InGaAs QW layers of 74 Å thickness corresponding to a room temperature photoluminescence peak at 1.546 $\mu$m. The InGaAsP barriers and waveguide layers were 132 Å and 645 Å thick, respectively, and were grown with a bandgap composition corresponding to the emission wavelength of 1.3 $\mu$m. Both ternary and quaternary layers were grown lattice matched to InP. The lower and upper InP confining layers were Si doped with $n = 10^{18}$ cm$^{-3}$ and Zn doped with $p = 5 \times 10^{17}$ cm$^{-3}$, respectively. An InGaAs contact layer Zn doped with $p = 10^{19}$ cm$^{-3}$ was grown on top. The broad area lasers were processed with a metal contact stripe of 100 $\mu$m width and cleaved with various cavity lengths in the range 350 - 700 $\mu$m. The $P-I$ characteristics were measured under pulsed conditions at a frequency of 1 kHz with pulse widths of 1 ms, to avoid heating of the MQW active layer.

## IV. Results and discussion

A typical $P-I$ plot of a SCH-MQW broad area laser is shown as the solid line in Fig. 2 for a cavity length of 700 $\mu$m. In a first analysis, we assumed $I_l = 0$ and determined $I_{th}$ and $dP/dI$ from the intersection and slope above threshold using equation (6), as shown with the dotted line of Fig. 2. The results obtained for 33 laser devices are shown in Figs. 3 and 4, where $j_{th}$ and $1/\eta_{ext}$ are plotted as a function of $1/L$ and $L$, respectively. The dotted lines in these figures are least square fits of the data points, which support equations (2) and (3) with $K = 0$ in equations (5) and (7), respectively. Since $g_0$ is independent of $K$, we can estimate its value from equation (2) using the semilogarithmic slope of $2.246 \times 10^{-2}$ cm shown in Fig. 3. If we assume $\Gamma_Z \approx 2 \times 10^{-4}\ L_Z(\AA)$ [6], such that $N_Z\Gamma_Z = 0.0888$, and $R_1(R_2) \approx 0.3$ for cleaved facets, we find $g_0 \approx 603.66\,\mathrm{cm}^{-1}$. This result is consistent with theoretical predictions obtained under the $k.p$ approximation for the evaluation of the material gain [11]. If we consider the dotted line in Fig. 4 to be representative of the data and use equation (3), we obtain $\eta_i = 0.4472$ and $\alpha_i = 30.11$ cm$^{-1}$. Then, assuming these values in equation (2), we find $j_0 = 59.15$ A/cm$^2$. The values found for $\alpha_i$ and $j_0$ agree with previous reports on similar MQW lasers and can be assumed hereafter, but $\eta_i$ is extremely low and unconsistent with previous assumptions [12]. Except for $L$ smaller than 50 $\mu$m, $\eta_i$ is expected to be always close to one [20].

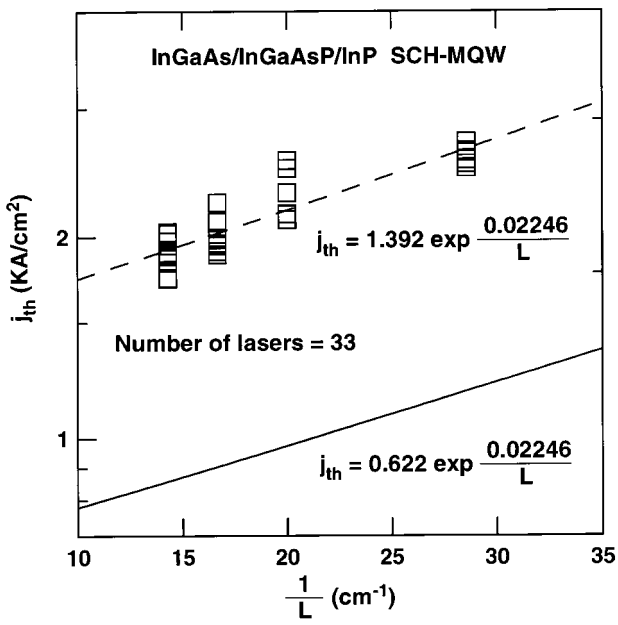


Figure 3. Threshold current densities of MQW broad area lasers presented as a function of $1/L$. The dashed and solid lines are least square fits for 33 lasers adjusted with equation (2) using $K = 0$ and 0.5528 in equation (5), respectively.

The $j_{th}$ data points shown in Fig. 3 within the range 1.7 - 3 KA/cm$^2$ as well as the low $\eta_{ext}$ values of Fig. 4, imply the existence of considerable current losses in the $P-I$ characteristics of these laser devices. The constant monotonic increase observed at low powers on the $P-I$ curve shown in Fig. 2 with a rounded shape near threshold, is consistent with a sizeable contribution of the spontaneous emission [16]. However, the presence of filamentation in the optical laser cavity cannot be simply inferred from the $P-I$ characteristics alone. We have thus undertaken measurements of the far field pattern and the emission spectra of similar MQW broad area lasers. The former presents an asymmetric and nonuniform distribution pattern which depends on the injected current, whereas the latter usually displays more than one family of longitudinal modes. These observations support the existence of filamentation in the optical cavity [9,27], and we have then employed the apparent leakage current model presented in section II, to describe the $P-I$ characteristics of our MQW lasers.

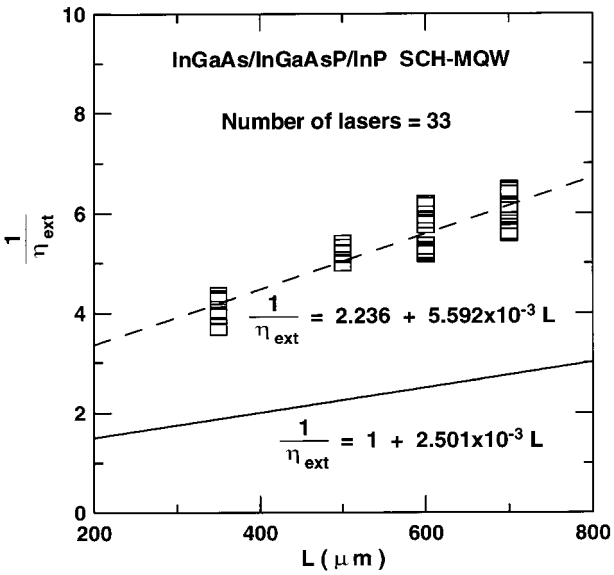


Figure 4. External quantum efficiencies of MQW broad area lasers presented as a function of $L$. The dashed and solid lines are least square fits for 33 lasers adjusted with equation (3) using $K = 0$ and 0.5528 in equation (7), respectively.

By assuming $\eta_i \approx 1$ and the values found above for $g_0$, $\alpha_i$ and $j_0$, we have determined the value of $K$ in equations (5) and (7) that matches equations (2) and (3). The results are shown as solid lines in Figs. 3 and 4 with $K = 0.5528$. This large value of $K$ implies a low injection efficiency for the measured $P - I$ characteristics, according to the factor $(1 - K)$ in equations (5) and (7), but it is consistent with previous assumptions of low current injection efficiencies due to filamentation in broad area lasers [28]. The $K$ parameter affects only the intercept at the ordinate of equation (2), in the same way as the low value found for $\eta_i$ above, whereas in equation (3), $K$ affects both the intersection at the ordinate as well as the slope.

Hence, we can estimate $dg/dn$ using the corrected values of $j_{th}$, which generate laser emission by filamentation in the MQW active region. Assuming $b = 2.55$ and $B_{eff} = 3 \times 10^{-20}$ cm$^{4.65}$/s in equation (9), and considering the expression shown for the solid line in Fig. 3 with $L = 350$ $\mu$m, we find $n_{th} \approx 2.14 \times 10^{18}$ cm$^{-3}$. From equation (11), we then obtain $dg/dn \approx 7.19 \times 10^{-16}$ cm$^2$. Following the same reasoning for $L = 700$ $\mu$m, we find $n_{th} \approx 1.89 \times 10^{18}$ cm$^{-3}$ and $dg/dn \approx 8.14 \times 10^{-16}$ cm$^2$. These results are in good agreement with our previous work [8] and with data reported by other investigators as discussed below. The increase of $dg/dn$ obtained in terms of $L$ results from the decrease of the mirror losses which reduce $j_{th}$. We can check the error obtained by neglecting $K$ in the evaluation of the threshold current density. If we consider the expression shown for the dotted line in Fig. 3 and equation (9) with $\eta_i \approx 1$, we find after the same analysis, the values $n_{th} \approx 2.94 \times 10^{18}$ cm$^{-3}$ and $dg/dn \approx 5.24 \times 10^{-16}$ cm$^2$, and $n_{th} \approx 2.59 \times 10^{18}$ cm$^{-3}$ and $dg/dn \approx 5.94 \times 10^{-16}$ cm$^2$, for $L = 350$ $\mu$m and $L = 700$ $\mu$m, respectively. We note that the values obtained for $n_{th}$ and $dg/dn$ are somewhat overestimated and underestimated, respectively. Thus, the value of $dg/dn$ is affected by $K$ only through the value of $n_{th}$ obtained with equation (9), since the value of $g_0$ derived from equation (2) does not change as long as $\eta_i$ remains constant.

We can now compare our results with data reported on similar lattice matched InGaAs/InGaAsP/InP MQW heterostructure lasers. Zah et al. [29] and Sasaki et al. [30] measured $dg/dn = 3.6 \times 10^{-16} - 6.7 \times 10^{-16}$ cm$^2$ and $dg/dn = 8.2 \times 10^{-16}$ cm$^2$, respectively, with 4 QWs. Fernier et al. [31] and Cavalier et al. [32] measured $dg/dn = 7.6 \times 10^{-16}$ cm$^2$ and $dg/dn = 4.8 \times 10^{-16} - 6.1 \times 10^{-16}$ cm$^2$, respectively, with 5 QWs. Tatham et al. [33] reported $dg/dn$ increasing from $1.9 \times 10^{-16}$ cm$^2$ to $7.7 \times 10^{-16}$ cm$^2$, as the number of QWs increased from 2 to 24. Seltzer et al. [34], reported $dg/dn = 6.1 \times 10^{-16}$ cm$^2$ for 16 QWs. Uomi et al. [35] measured $dg/dn = 5.5 \times 10^{-16}$ cm$^2$, $8.3 \times 10^{-16}$ cm$^2$ and $1 \times 10^{-15}$ cm$^2$, in a heterostructure with 5, 10 and 15 QWs, respectively. Most of these results were obtained with the small signal modulation technique in devices of small cavity lengths. The effect of leakage currents have not been considered, but a low frequency roll-off observed at higher optical powers can decrease somewhat the value measured for $dg/dn$ [6]. This might explain in part our higher values compared to laser devices reported with similar number of QWs. However, different techniques have been shown to induce slightly different results with the same MQW heterostructure [32]. Other possible differences arise from unknown values of $\eta_i$ as well as different values of $\alpha_i$ which depend on the laser strucuture. Moreover, there are uncertainties regarding

the value of $g_0$ in InGaAs/InGaAsP/InP MQW heterostructures, since somewhat lower and higher values were also reported [11,36].

## V. Conclusion

We have analysed the differential gain of MQW broad area lasers emitting at the wavelength of 1.55 $\mu$m, taking into account the carrier density losses produced by filamentation in the optical cavity. The differential gain was determined from measurements of the threshold current density including the losses due to the nonuniform laser emission as an apparent leakage current effect in the $P-I$ characteristics. The broad area SCH-MQW lasers were grown by MOCVD and incorporated an InGaAs/InGaAsP/InP heterostructure in the active layer. For cavity lengths of 350 $\mu$m and 700 $\mu$m, we have found the values $dg/dn \approx 7.19\times10^{-16}$ cm$^2$ and $8.14\times10^{-16}$ cm$^2$, respectively, which are consistent with previous results.

## Acknowledgements

The authors would like to thank L.K.Horiuchi for technical assistance during the MOCVD growth.

## References

1. Y. Arakawa and A. Yariv, IEEE J. Quantum Electron. **21**, 1666 (1985).
2. I. Suemune, IEEE J. Quantum Electron. **27**, 1149 (1991).
3. K. Uomi, T. Tsuchiya, H. Nakano, M. Aoki, M. Suzuki and N. Chinone, IEEE J. Quantum Electron. **27**, 1705 (1991).
4. S.J. Wang, L.J.P. Ketelsen, V.R. McCrary, Y. Twu, S.G. Napholtz and W.V. Werner, IEEE Photon. Technol. Lett. **2**, 775 (1990).
5. M. Blez, D. Mathoorasing, C. Kazmierski, M. Quillec, M. Gilleron, J. Landreau and H. Nakajima, IEEE J. Quantum Electron. **29**, 1676 (1993).
6. M.T. Furtado, E.J.T. Manganote, A.C.G. Bordeaux-Rêgo, F. Steinhagen, H. Janning and H. Burkhard, Braz. J. Phys. **27**, 411 (1997). This issue.
7. J.E. Bowers, Sol. St. Electron. **30**, 1 (1987).
8. M.T. Furtado, W. Carvalho Jr., C.M.A. Coghi, E.J.T. Manganote and A.C.G. Bordeaux- Rêgo, Rev. Fis. Apl. Instr., vol. **11**, (1996). In press.
9. Y. Lam, E. Espinosa, D. Nichols, L. Davis and P. Bhattacharya, IEEE J. Quantum Electron. **29**, 1018 (1993).
10. S.Y. Hu, D.B. Young, A.C. Gossard and L.A. Coldren, IEEE J. Quantum Electron. **30**, 2245 (1994).
11. T.A. DeTemple and C.M. Herzinger, IEEE J. Quantum Electron. **29**, 1246 (1993).
12. M.T. Furtado, Braz. J. Phys. **24**, 466 (1994).
13. . J.Z. Wilcox, G.L. Peterson, S. Ou, J.J. Yang, M. Jansen and D. Schechter, J. Appl. Phys. **64**, 6564 (1988).
14. H. Hirayama, Y. Miyake and M. Asada, IEEE J. Quantum Electron. **28**, 68 (1992).
15. K. Sang-Bae, H. Yong-Su and D. Man-Hee, Electron. Lett. **29**, 1791 (1993).
16. M. Asada, in *Handbook of Semiconductor Lasers and Photonic Integrated Circuits,* Eds. Y. Suematsu and A.R. Adams (Chapman & Hall, London, 1994), p.236.
17. A.R. Adams, M. Asada, Y. Suematsu and S. Arai, Japan. J. Appl. Phys. **19**, L261 (1980).
18. G.P. Agrawal and N.K. Dutta, in *Semiconductor Lasers*, 2nd edition (Van Nostrand Reinhold, New York, 1993), chap.2.
19. H. Hirayama, J. Yoshida, Y. Miyake and M. Asada, IEEE J. Quantum Electron. **30**, 54 (1994).
20. P.R. Claisse and G.W. Taylor, Electron. Lett. **28**, 1991 (1992).
21. G.H.B. Thompson, Opto-electronics **4**, 257 (1972).
22. A.H. Paxton and G.C. Dente, J. Appl. Phys. **70**, 2921 (1991).
23. J.R. Marciante and G.P. Agrawal, IEEE J. Quantum Electron. **32**, 590 (1996).
24. R.J. Lang, A.G. Larsson and J.G. Cody, IEEE J. Quantum Electron. **27**, 312 (1991).
25. B. Fernier, P. Brosson, J.P. Jicquel and J. Benoit, IEE Proc. J **134**, 27 (1987).
26. J. Jacquet, P. Brosson, A. Olivier, A. Perales, A. Bodere and D. Leclerc, IEEE Photon. Technol. Lett. **2**, 620 (1990).
27. H.C. Casey Jr. and M.B. Panish, in *Heterostructure Lasers Part B*, Eds. Y.H. Pao and P. Kelley (Academic Press, New York, 1978), chap. 7.
28. O. Hess, S.W. Koch and J.V. Moloney, IEEE J. Quantum Electron. **31**, 35 (1995).
29. C.E. Zah, R. Bhat, S.G. Menocal, F. Favire, N.C. Andreakis, M.A. Koza, C. Caneau, S.A. Scwarz, Y. Lo and T.P. Lee, IEEE Photon. Technol. Lett. **2**, 231 (1990).

30. T. Sasaki, H. Yamazaki, N. Henmi, H. Yamada, M. Yamaguchi, M. Kitamura and I. Mito, J. Lightwave Technol. **8**, 1343 (1990).
31. B. Fernier, L. Goldstein, A. Olivier, A. Perales, C. Stark and J. Benoit, Proc. 15th ECOC (Sweden) WeB14-6, pp.264-267 (1989).
32. M. Cavalier, J.M. Lourtioz, J.M. Xie, L. Chusseau, B. DeCremoux, M. Krawkowski and D. Rondi, Electron. Lett. **27**, 513 (1991).
33. M.C. Tatham, I.F. Lealman, C.P. Seltzer, L.D. Westbrook and D.M. Cooper, IEEE J. Quantum Electron. **28**, 408 (1992).
34. C.P. Seltzer, S.D. Perrin, M.C. Tatham and D.M. Cooper, Electron. Lett. **28**, 63 (1992).
35. K. Uomi, M. Aoki, T. Tsuchiya, M. Suzuki and N. Chinone, IEEE Photon. Technol. Lett. **3,** 493 (1991).
36. C. Kazmierski, A. Ougazzaden, M. Blez, D. Robein, J. Landreau, B. Sermage, J.C. Bouley and A. Mircea, IEEE J. Quantum Electron. **27**, 1794 (1991).